P H Y S I C A L   R E V I E W   L E T T E R S

Spin Dynamics in the Carrier-Doped $S = \frac{1}{2}$ Triangular Lattice of $Na_xCoO_2 \cdot yH_2O$

F. L. Ning,[1] T. Imai,[1,2] B. W. Statt,[3] and F. C. Chou[4]

[1]*Department of Physics and Astronomy, McMaster University, Hamilton, Ontario L8S 4M1, Canada*
[2]*Canadian Institute for Advanced Research, Toronto, Ontario M5G 1Z8, Canada*
[3]*Department of Physics, University of Toronto, Toronto, Ontario M5S 1A7, Canada*
[4]*Center for Materials Science and Engineering, MIT, Cambridge, Massachusetts 02139, USA*

We probed the local electronic properties of the mixed-valent Co^{+4-x} triangular lattice in $Na_xCoO_2 \cdot yH_2O$ by ^{59}Co NMR. We observed two distinct types of Co sites for $x \gtrsim \frac{1}{2}$, but the valence seems averaged out for $x \sim \frac{1}{3}$. Local spin fluctuations exhibit qualitatively the same trend down to ~ 100 K regardless of the carrier concentration x, and hence the nature of the electronic ground state. A canonical Fermi-liquid behavior emerges below ~ 100 K only for $x \sim \frac{1}{3}$.

There is widespread speculation that the water-intercalated $Na_{0.3}CoO_2 \cdot 1.3H_2O$ ($T_c \sim 4.5$ K) [1] represents the first example of the long-sought resonating valence bond (RVB) [2] superconductor in a carrier-doped $S = \frac{1}{2}$ *triangular lattice* [3]. The symmetry of the order parameter appears to be unconventional [4]. The parent compound of the superconducting $Na_{0.3}CoO_2 \cdot 1.3H_2O$ is a mixed-valent Na_xCoO_2 with sheets of Co^{4+} ions ($S = \frac{1}{2}$) arranged in a triangular lattice. Na^+ ions dope additional electrons with probability x [5]. The electronic and magnetic phase diagram of Na_xCoO_2 is quite rich [5–9] because of the interplay between doped carriers and inherently frustrated spins on triangular lattice (see Fig. 1), and includes commensurate antiferromagnetism ($x = 0.82$ [8] and 0.5 [9]), spin-density wave (SDW) ($x \sim 0.75$ [7]), and Fermi-liquid state ($x \sim 0.31$ [6]). Among the key issues are: Does charge order(s) exist in carrier-doped Co triangular lattice, as hinted by earlier magnetic resonance [8–10] and bulk studies [6]? How do Co spin fluctuations evolve with x? Is the ground state of $\frac{1}{3}$ doped triangular lattice a Fermi-liquid or ferromagnetic [3]? Do exotic phases (e.g., pseudogap [11] and stripe [12]) exist, in analogy with high T_c cuprates?

In this Letter, we will shed new light on the anomalous behavior of the carrier-doped Co triangular lattice in $Na_xCoO_2 \cdot yH_2O$ based on systematic ^{59}Co NMR measurements. The main thrust of our approach is that we can *separately* observe and characterize Co ions in different valence states. From the NMR line shape (Fig. 2), local uniform spin susceptibility (as measured by ^{59}Co NMR Knight shift ^{59}K, Fig. 3), and local spin fluctuations (as measured by nuclear spin-lattice relaxation rate $\frac{1}{T_1}$, Fig. 4), we establish that two types of mutually coupled Co ions with different local electronic properties exist in $x \geq 0.5$. Furthermore, we show that low-frequency spin fluctuations exhibit qualitatively the same trend down to ~ 100 K for all Na concentrations x, despite their different electronic ground states. A canonical Fermi-liquid

behavior emerges below 100 K only for $x = 0.3$, and water intercalation enhances spin fluctuations near T_c.

^{59}Co nuclei have spin $I = \frac{7}{2}$ (nuclear gyromagnetic ratio $\gamma_n = 10.053$ MHz/T), and seven NMR transitions from the $I_z = m$ to $m + 1$ state are expected for each different type of Co site [13]. We show representative line shapes observed in the external magnetic field $H_{ext} = 8$ T in Fig. 2. All samples are single crystals [14] except for $x = 0.72$; the latter is a ceramic sample synthesized by the standard *fast-heating* method [15], and magnetically aligned in Stycast 1266. The line shapes for $x = 0.75$, 0.72, 0.67, and 0.5 clearly establish the presence of at least two different types of ^{59}Co NMR lines. They have different central resonance frequencies, e.g., $\nu_{-1/2,+1/2} \sim 82$ MHz at A' sites and ~ 86 MHz at B' sites in $Na_{0.72}CoO_2$. In addition, the splitting, ν_a, between the central and satellite transitions due to nuclear quadrupole interaction with the local electric-field gradient (EFG) [13] is different, e.g., $\nu_a \sim 560$ kHz at A' sites and $\nu_a \sim 650$ kHz at B' sites.
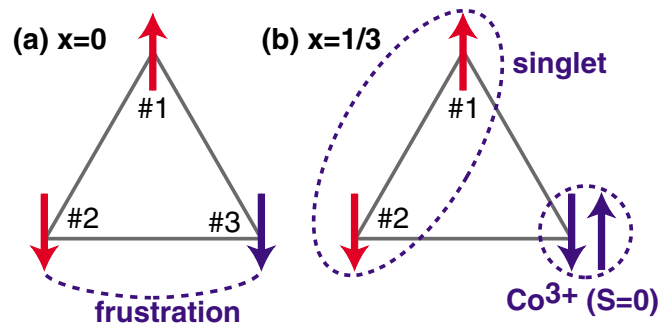

FIG. 1 (color online). (a) Schematics of the undoped ($x = 0$) Co^{4+} triangular lattice with $S = \frac{1}{2}$. When the nearest-neighbor exchange interaction J tends to align two $S = \frac{1}{2}$ spins (#1 and #2) in an antiparallel configuration, frustration would result for spin #3. (b) For finite values of x ($x = \frac{1}{3}$ in this panel), extra electrons could help local-singlet formation, and alter spin correlations dramatically.
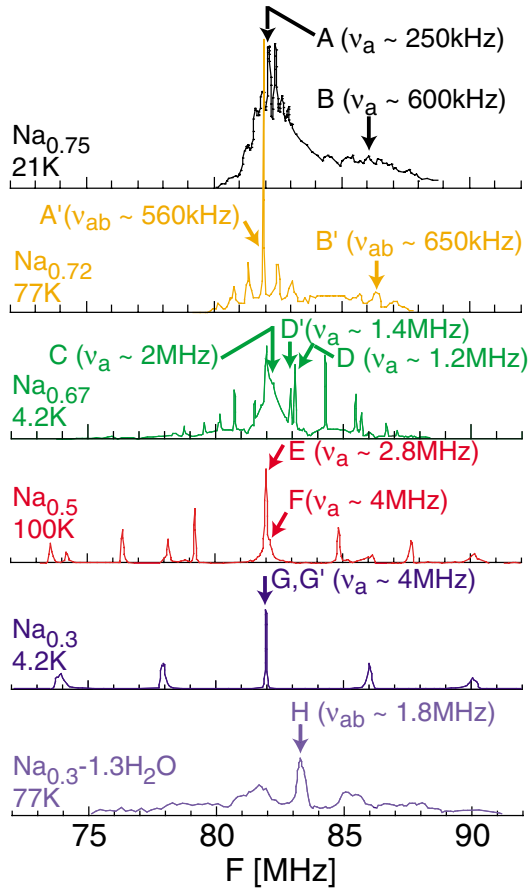
FIG. 2 (color online). ^{59}Co NMR line shape with $H_{ext} = 8$ T applied along a axis. (The line shapes for $Na_{0.72}CoO_2$ and $Na_{0.3}CoO_2 \cdot 1.3H_2O$ were obtained with H_{ext} applied within the ab plane for aligned ceramics and single crystals, respectively. The line shapes for $x = 0.75$ and 0.72 are corrected for T_2.) The arrows indicate the central transition $\nu_{-1/2,+1/2}$ at various Co sites. For $x = 0.75$, 0.72, and 0.67, ^{23}Na NMR line was superposed above ~ 88 MHz. Some of the furthest satellite transitions are not shown.

In the absence of hyperfine interactions with Co electrons, the ^{59}Co NMR frequency would be $\gamma_n H_{ext} = 80.4$ MHz in $H_{ext} = 8$ T. It is primarily the hyperfine magnetic field at each Co site that shifts the central resonance frequency $\nu_{-1/2,+1/2}$, and the former has a linear relation to the local magnetic susceptibility χ^i_{spin} at the i-th Co site. Generally, one can gain information on χ^i_{spin} through the NMR Knight shift ^{59}K $= (\nu_{-1/2,+1/2} - \gamma_n H_{ext})/\gamma_n H_{ext}$ [13] as presented in Fig. 3 [16], where

$$^{59}\text{K} = {}^{59}\text{K}_{spin} + {}^{59}\text{K}_{orb} = \sum_{i=0\sim6} H_i \chi^i_{spin} + {}^{59}\text{K}_{orb}. \quad (1)$$

^{59}K$_{spin}$ is the spin contribution to the NMR Knight shift, H_0 is the hyperfine interaction between the observed Co nuclear spin and the Co electron spin at the same site, and $H_{1\sim6}$ represents the hyperfine interaction with electron spins at six nearest-neighbor Co sites. The orbital contri-
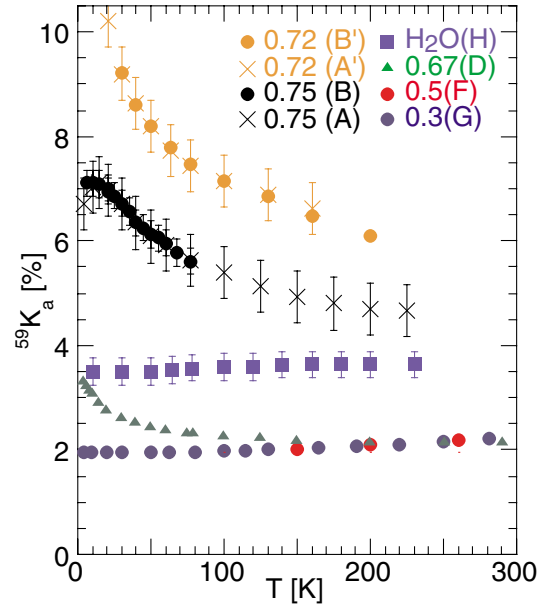

FIG. 3 (color online). The ^{59}Co NMR Knight shifts ^{59}K$_a$ at B, B', D, F, G, and H sites. (Note that ^{59}K$_{orb} \sim 2$–3% is *not* subtracted.) Also plotted are ^{59}K$_c$ measured at A and A' sites scaled to match with B and B' sites (see the main text).

bution is usually temperature independent, and is estimated to be ^{59}K$_{orb} = (2 \sim 3)$% below 250 K based on preliminary K vs χ analysis [17].

In Fig. 4, we summarize $\frac{1}{T_1 T}$, the ^{59}Co nuclear spin-lattice relaxation rate $\frac{1}{T_1}$ divided by temperature T. $\frac{1}{T_1 T}$ measures the low-frequency spectral weight of the local Co spin fluctuations at the experimental frequency $\nu_n = 78 \sim 86$ MHz (depending on the particular transition we employ). Theoretically, the spin contributions to $\frac{1}{T_1 T}$ may be written using the imaginary part of the Co dynamical electron-spin-susceptibility $\chi''(\mathbf{q}, \nu_n)$ as [18],

$$\frac{1}{T_1 T} = \frac{2\gamma_n^2 k_B}{g^2 \mu_B^2} \sum_{\mathbf{q}} |A(\mathbf{q})|^2 \frac{\chi''(\mathbf{q}, \nu_n)}{\nu_n}, \quad (2)$$

where $A(\mathbf{q}) = H_0 + \sum_{i=1\sim6} H_i e^{i\mathbf{q}\mathbf{r}_i}$ is the wave vector $\mathbf{q}$-dependent hyperfine *form factor* [18,19].

It is very important to realize that the spin contribution to the Knight shift show identical temperature dependence at two different Co sites in $Na_{0.75}CoO_2$ (A and B sites), as well as in $Na_{0.72}CoO_2$ (A' and B' sites), despite the factor 6 to 8 difference in their magnitude. To underscore this point, in Fig. 3 we plotted $6.05 \times [^{59}$K$_c(A) - 1.1\%]$ and $8.43 \times [^{59}$K$_c(A') - 1.65\%]$ to match with ^{59}K$_a$ at B and B' sites, respectively. In Fig. 4, we also demonstrate that $\frac{1}{T_1 T}$ at B and B' sites show identical behavior with that at A and A' sites, respectively [20]. These results are not consistent with a simple phase-separation picture, and imply that the strongly magnetic B and B' sites are electronically coupled with the less magnetic A and A'

sites, respectively. Furthermore, the ratio of the integrated NMR intensity between the strongly magnetic (B and B' sites) and less magnetic Co sites (A and A' sites) is consistent with $(1 - x){:}x$ after careful corrections for the fast transverse relaxation time T_2 at the B and B' site. These findings strongly suggest that a charge order leads to two mutually coupled Co sites: A and A' sites are less magnetic Co^{3+}-like ions with $S \sim 0$, while B and B' sites are strongly magnetic Co^{4+}-like ions with $S \sim \frac{1}{2}$.

In passing, notice that the saturation below ~ 20 K of $^{59}K(A)$ and $^{59}K(B)$ (both in Fig. 3) and SQUID data (not shown) in our $Na_{0.75}CoO_2$ is consistent with the SQUID data reported by Foo *et al.* [6] for their $Na_{0.75}CoO_2$ sample with accurately calibrated Na content. Our NMR and SQUID data showed no evidence for a bulk magnetic phase transition in this $Na_{0.75}CoO_2$ crystal. On the other hand, an earlier muon spin resonance (μSR) work reported [7] a SDW phase transition below ~ 20 K for $\sim 20\%$ volume fraction of a ceramic "$Na_{0.75}CoO_2$" sample prepared by *fast-heating* method [15]. Interestingly, our $Na_{0.72}CoO_2$ ceramic sample, prepared by the same *fast-heating* method, showed a continuous increase of SQUID data through ~ 20 K following a Curie-Weiss behavior, and we found a variety of NMR signatures of a magnetic instability (e.g., a dramatic magnetic NMR line broadening of B' line below ~ 30 K, accompanied by temperature-dependent line splitting of A' line and Na NMR line [17]). The Na content of our ceramic sample was determined to be 0.72 ± 0.02 based on the $c-$ axis lattice constant, which is a monotonous function of Na content [6]. The complete details will be reported elsewhere [17].

In the antiferromagnetic phase $Na_{0.5}CoO_2$ [8], we also observed two types of Co NMR signals, E sites and F sites, with the integrated-intensity ratio 0.5:0.5. This is again consistent with a charge order, but with a geometrical configuration different from $Na_{0.72-0.75}CoO_2$. Based on the magnitude of $\frac{1}{T_1T}$, we may identify the E and F sites as the weakly and strongly magnetic Co sites, respectively. However, the valence of E and F sites may not be very different from the nominal averaged value of 3.5, as the difference in the magnitude of $\frac{1}{T_1T}$ is at most ~ 3 and less dramatic than the case of $Na_{0.72-0.75}CoO_2$. We also found that the ^{59}Co NMR satellite line shape begins to show additional line splitting below 88 K [17] where SQUID data exhibit a kink [6,14]. This suggests that the configuration of charge order changes below 88 K. We note that a recent structural study at 3.5 K suggests a zigzag chain structure with two distinct Co sites [21]. A large distribution in the magnitude of $\frac{1}{T_1T}$ prevented us from defining it properly below ~ 88 K.

In metallic $Na_{0.67}CoO_2$, we observed only sharp D and D' lines above ~ 30 K, and their NMR properties were very similar. With decreasing temperature, broad C sites emerge while the linewidth of the D and D' sites broadens. $\frac{1}{T_1T}$ at D sites is similar to that at the weakly magnetic A
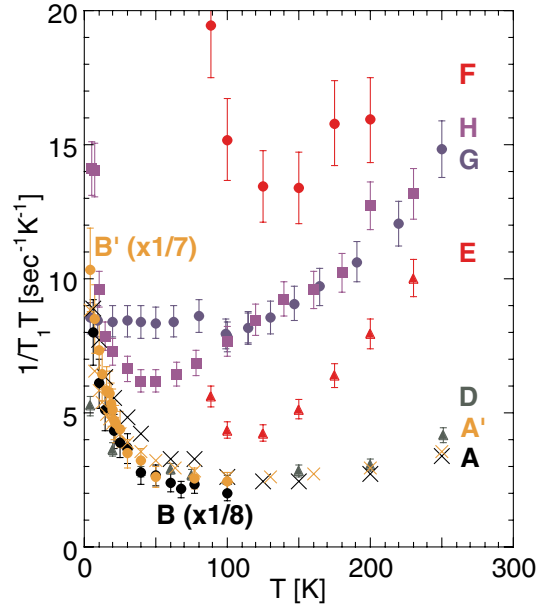

FIG. 4 (color online).   The temperature dependence of $\frac{1}{T_1T}$.

sites in $Na_{0.75}CoO_2$. The ratio of the integrated intensity between C and D, D' sites is not consistent with 0.33:0.67 nor 0.67:0.33. The Co sites with magnetic moments may be missing in the $Na_{0.67}CoO_2$ line shape due to their fast relaxation times.

In contrast with the results for $x \gtrsim 0.5$, we have detected essentially only one class of ^{59}Co NMR lines, G and G', in metallic $Na_{0.3}CoO_2$ at 4.2 K. ν_a, ^{59}K, and $\frac{1}{T_1T}$ were nearly identical at both sites. Thus the valence of all Co ions in the ground state of $x \sim \frac{1}{3}$ doped $Na_{0.3}CoO_2$ seems averaged out. The special character of the electronic state at the $x \sim \frac{1}{3}$ doping may be induced by the geometry, as dynamic singlet formation would be energetically advantageous; see Fig. 1(b). However, we cannot rule out the possibility that changes in the nature and extent of Na^+ vacancy order may be driving the changes of electronic properties across $x = 0.5$.

Now we turn our attention to the low-frequency Co spin dynamics. One of the most interesting findings of this study is that $\frac{1}{T_1T}$ shows qualitatively the same decrease with temperature down to ~ 100 K at all types of Co sites in all concentrations, regardless of the nature of the electronic properties below ~ 100 K and of the behavior of ^{59}K (i.e., the $\mathbf{q} = \mathbf{0}$ behavior of χ^i_{spin}). For example: $\frac{1}{T_1T}$ at A, A', and D sites decreases $\sim 30\%$ from 250 K to 100 K, where χ^i_{spin} shows an increase following a Curie-Weiss law; in $x = 0.3$, $\frac{1}{T_1T}$ decreases $\sim 40\%$ in the same temperature range while χ^i_{spin} also *decreases*. Even more interesting is the fact that $\frac{1}{T_1T}$ above 100 K at G sites in $Na_{0.3}CoO_2$ is roughly the average of $\frac{1}{T_1T}$ at weakly magnetic E sites and strongly magnetic F sites in $Na_{0.5}CoO_2$. Furthermore,   our   preliminary   results   for   water-

intercalated, superconducting single-crystal $Na_{0.3}CoO_2 \cdot 1.3H_2O$ show identical $\frac{1}{T_1T}$ to that of $Na_{0.3}CoO_2$ above ~ 100 K. The identical behavior indicates that the weaker inter-Co layer coupling along the c axis caused by water intercalation does not affect the behavior of Co spin fluctuations above ~ 100 K.

Thus our $\frac{1}{T_1T}$ results establish qualitatively the same suppression in the carrier-doped $S = \frac{1}{2}$ triangular lattice with a comparable temperature scale(s) of the order of ~ 100 K or higher, regardless of the carrier concentration x and the interlayer coupling. Interestingly, the intralayer Co-Co exchange interaction is estimated to be $J = 140 \sim 280$ K for $Na_xCoO_2 \cdot yH_2O$ by Wang $et\ al.$ [3]. This reminds us that the Cu spin-lattice relaxation rate in the high-T_c cuprate $La_{2-x}Sr_xCuO_4$ exhibits a universal value set entirely by the Cu-Cu exchange interaction $J \sim 1500$ K above ~ 500 K [22]. Perhaps J is the single dominant parameter of $\frac{1}{T_1T}$ in the present case, too.

According to Eq. (2), our $\frac{1}{T_1T}$ data imply that the **q** integral of the low-frequency components of Co spin fluctuations, weighted with the form factor $|A(\mathbf{q})|^2$, decreases with temperature down to ~ 100 K. Since the total magnetic moment must be conserved, a possible scenario is that some spectral weight is being shifted to higher energies, in analogy with the pseudogap behavior in under-doped high T_c cuprates [11]. Alternatively, the growth of the short-range order of Co spins below $T \sim J$ may result in the pileup of a considerable fraction of the spectral weight of $\chi''(\mathbf{q}, \nu_n)$ to a **q** region where the form factor $|A(\mathbf{q})|^2$ happens to be small [23].

Surprisingly, despite qualitatively the same trend in spin dynamics for all concentrations x down to ~ 100 K, both $\frac{1}{T_1T}$ and ^{59}K level off below ~ 100 K only for $x = 0.3$, i.e., Korringa behavior [13]. This evidences for the emergence of a low-temperature canonical Fermi-liquid behavior for $x \sim \frac{1}{3}$ below ~ 100 K, and is consistent with the emergence of $\sim T^2$ behavior of resistivity observed only for $x \sim \frac{1}{3}$ below ~ 30 K [6]. The large low-temperature specific heat $\gamma \sim 10$ mJ/K^2 mol implies a substantial mass enhancement by a factor $4 \sim 7$ [24]. Quite remarkably, water intercalation alters the temperature dependence of $\frac{1}{T_1T}$ for the $x \sim \frac{1}{3}$ doping below and only below ~ 100 K. Somehow the reduced interlayer coupling between Co sheets appears to introduce a new temperature (and/or energy) scale in the low-temperature Fermi-liquid state in $x \sim \frac{1}{3}$.

To conclude, we demonstrated the presence of two types of Co sites in the carrier-doped Co triangular lattice of $Na_xCoO_2 \cdot yH_2O$ for $x \geq 0.5$ by probing the Co layers directly with ^{59}Co NMR. The temperature dependences of ^{59}K and $\frac{1}{T_1T}$ suggest these sites are electronically coupled to each other. We also showed semiquantitatively the same trend of spin fluctuations above ~ 100 K for a variety of carrier concentrations from $x = 0.3$ to 0.75 with $y = 0$, and for varying strength of interlayer cou-

pling for a fixed $x = 0.3$ (i.e., $y = 0$ and $y = 1.3$). Our $\frac{1}{T_1T}$ results suggest the presence of a certain energy scale that shows little dependence on x and y. We also demonstrated that a canonical Fermi-liquid behavior emerges at low temperatures only for $x \sim \frac{1}{3}$ but water intercalation alters the low-temperature spin dynamics.

[1] K. Takada $et\ al.$, Nature (London) **422**, 53 (2003).

[2] P. W. Anderson, Science **235**, 1196 (1987).

[3] G. Baskaran, Phys. Rev. Lett. **91**, 097003 (2003); D. J. Singh, Phys. Rev. B **68**, 020503 (2003); B. Kumar and B. S. Shastry, Phys. Rev. B **68**, 104508 (2003); Q.-H. Wang, D.-H. Lee, and P. A. Lee, Phys. Rev. B **69** 092504 (2004); O. I. Motrunich and P. A. Lee, Phys. Rev. B **70** 024514 (2004); T. Koretsune and M. Ogata, Phys. Rev. Lett. **89**, 116401 (2002).

[4] T. Fujimoto $et\ al.$, cond-mat/0307127; K. Ishida $et\ al.$, cond-mat/0308506; T. Waki $et\ al.$, cond-mat/0306036.

[5] I. Terasaki $et\ al.$, Phys. Rev. B **56**, R12685 (1997); Y. Ando $et\ al.$, Phys. Rev. B **60**, 10580 (1999); Y. Wang $et\ al.$, Nature (London) **423**, 425 (2003); S. Y. Li $et\ al.$, Phys. Rev. Lett. **93** 056401 (2004).

[6] M. L. Foo $et\ al.$, Phys. Rev. Lett. **92** 247001 (2004).

[7] J. Sugiyama $et\ al.$, Phys. Rev. B **68** 134423 (2003).

[8] Y. J. Uemura $et\ al.$ (to be published).

[9] S. Bayrakci $et\ al.$, Phys. Rev. B **69** 100410 (2004).

[10] R. Ray $et\ al.$, Phys. Rev. B **59**, 9454 (1999); M. Itoh $et\ al.$, Physica B (Amsterdam) **281-282**, 516 (2000); J. L. Gavilano $et\ al.$, Phys. Rev. B **65** 214202 (2002); P. Carretta $et\ al.$, Phys. Rev. B **70** 024409 (2004); I. R. Mukhamedhin, cond-mat/0402074.

[11] T. Timusk and B. Statt, Rep. Prog. Phys. **62**, 61 (1999).

[12] J. M. Tranquada $et\ al.$, Nature (London) **375**, 561 (1995).

[13] C. P. Slichter, $Principles\ of\ Magnetic\ Resonance$ (Springer-Verlag, Berlin, 1990).

[14] F. C. Chou $et\ al.$, Phys. Rev. Lett. **92** 157004 (2004); F. C. Chou $et\ al.$, Phys. Rev. B **70** 144526 (2004).

[15] T. Motohashi $et\ al.$, Appl. Phys. Lett. **79**, 1480 (2001).

[16] $^{59}K(C)$ and $^{59}K(E)$ (both $\sim 2\%$) were difficult to measure due to their proximity to other lines.

[17] F. L. Ning $et\ al.$ (to be published).

[18] T. Moriya, J. Phys. Soc. Jpn. **18**, 516 (1963).

[19] B. S. Shastry, Phys. Rev. Lett. **63**, 1288 (1989).

[20] Superposition of the intense NMR signals from A and A' sites made accurate measurements for B and B' sites impossible at higher temperatures.

[21] Q. Huang $et\ al.$, cond-mat/0402255.

[22] T. Imai $et\ al.$, Phys. Rev. Lett. **70**, 1002 (1993).

[23] Notice, however, that the **q** dependence of $|A(\mathbf{q})|^2$ is sensitive to the hyperfine couplings H_i, which in turn are sensitive to charge-order configurations for different x.

[24] J. H. Cho $et\ al.$ (unpublished).